A DIFFUSION TENSOR IMAGING TRACTOGRAPHY ALGORITHM BASED ON NAVIER-STOKES FLUID MECHANICS

Nathan S. Hageman, David W. Shattuck, Katherine Narr, Arthur W. Toga

Laboratory of NeuroImaging, Department of Neurology UCLA School of Medicine, Los Angeles, CA

ABSTRACT

We introduce a method for estimating regional connectivity in diffusion tensor magnetic resonance imaging (DT-MRI) based on a fluid mechanics model. We customize the Navier-Stokes equations to include information from the diffusion tensor and simulate an artificial fluid flow. The velocity vector field of this fluid construct is then used as a connectivity metric. We generate probable connection paths by maximizing the fluid velocity along a path between two regions of interest while constraining its bending energy. Our method is based on a second-order nonlinear partial differential equation (PDE) and incorporates local anisotropy and similarity measurements into a viscosity term, which extends previous linear first-order methods. We tested our algorithm on a digital DTI phantom. Our method was able to correctly segment the structure of the phantom with various levels of noise, despite local distortion of the image pattern. We applied our method to DTI volumes from a normal human subject. Seed points were chosen along the corticospinal tracts, white matter regions with well-known connectivity. Our method produced paths that were consistent with both known anatomy and directionally encoded color (DEC) images of the DTI volumes. Applying our method to a digital phantom that simulates discrete white matter lesions, we also demonstrate that the fluid velocity field around areas of simulated localized white matter disruption becomes dampened and turbulent compared to the heat flow field from a first order PDE method. This provides a means for identifying lesion position from the fluid velocity field.

1. INTRODUCTION

Diffusion tensor magnetic resonance imaging (DT-MRI) is used for the assessment of functional white matter tracts in the brain based on directional variations in the bulk diffusion of water [1]. DT-MRI provides information non-invasively about white matter integrity and orientation *in vivo* without the use of contrast agents [2]. DT-MRI uses at least 6 independent magnetic gradient directions to construct a symmetric tensor at each voxel which estimates the local directional dependence of diffusion. Diagonalization of this tensor produces a set of eigenvectors and eigenvalues, which can be used to calculate rotationally invariant scalar quantities. In this paper, we use the fractional anisotropy, a measure of the voxel's deviation from purely isotropic diffusion, and the lattice index, a measure of the local coherence of diffusion direction [2].

These scalar quantities are characteristically high in white matter and can provide a basis for white matter segmentation. However, they fail to provide information about regional connectivity. This has motivated the creation of DTI tractography methods that use the diffusion tensor field to estimate information about the brain's regional connectivity. Early work in this area focused on generating tract representations based on following voxel-wise the local major diffusion direction [3].

PDE-based DTI tractography algorithms model the dynamics of some entity through the tensor field to produce a metric of connectivity. An advantage of these methods is that they use the full diffusion tensor and thus retain the information in the minor diffusion directions. Previous work has simulated a diffusion process modeled by the first order heat equation. Batchelor *et al.* generated connection-based probabilities using a metric based on time of arrival of the heat propagation front [4] and were the first to implement an additional convection term in the heat equation [5]. O'Donnell *et al.* generated probability maps using a metric based on the total heat flow along a path in the heat flux vector field [6].

We present a new method that extends the probabilistic first order PDE methods by implementing a model based on the second order non-linear Navier-Stokes equations. Our method uses an artificial fluid modeled on local anisotropy and similarity information and simulates its flow through points in the DTI volume. The resulting fluid velocity vector field represents the local directionality of diffusion in the underlying DTI image. Using this fluid velocity field as a metric of connection strength between brain regions, we generate probable connection paths by maximizing the flow velocity. We apply our method to DT-MRI volumes from normal human subjects and to digital DTI phantoms to validate our approach.

2. METHODS

Our algorithm uses the physics described by the Navier-Stokes equations to model fluid flow through a pressure field that is derived from the diffusion tensor field. We seed a known volume of fluid, simulate its flow through the pressure field, and then use the corresponding fluid velocity vector field as a basis for estimating regional connectivity.

2.1. Model Construction

The Navier-Stokes equations describe the flow of a viscous fluid through a pressure tensor field. In a generalized coordinate system, the equations are

$$\frac{\partial \rho v_i}{\partial t} + \nabla \cdot (\rho v_i \overline{\mathbf{v}}) = \nabla \cdot (\mu \nabla v_i) - \nabla \cdot \overline{\mathbf{P}}, \qquad (1)$$

where $\overline{\mathbf{v}} = \{v_i\} = \{u, v, w\}$ in $\mathbb{R}^3$, μ is the viscosity, ρ is the fluid density, and $\overline{\mathbf{P}}$ is the pressure tensor.

Our algorithm uses an artificial fluid whose viscosity is derived from measurements taken from the diffusion tensor image. The

This work was funded by the National Institutes of Health through the NIH Roadmap for Medical Research, Grant U54 RR021813 entitled Center for Computational Biology (CCB). Information on the National Centers for Biomedical Computing can be obtained from http://nihroadmap.nih.gov/bioinformatics.

viscous forces are modeled as the product of the local fractional anisotropy, FA, which describes the degree of directionality of the local diffusion, and the lattice index, LI, which describes the local similarity in diffusion direction:

$$\mu = k(1 - (FA \times LI)), \tag{2}$$

where k is a proportionality constant that depends on the DTI image parameters. The viscous force therefore has the property of restricting fluid flow in areas of low anisotropy or coherence, such as gray matter and CSF.

Because we use fluid velocity as a metric of connection strength, it is imperative that the pressure on the fluid, which governs the flow dynamics in our model, is related to the underlying diffusion process. Therefore, we derive the pressure field for our model by considering the diffusion tensor at each voxel as a pressure tensor over the volume of fluid in that voxel. This represents a mapping from diffusion to pressure space,

$$\overline{\mathbf{D}} = \begin{pmatrix} D_{xx} & D_{xy} & D_{xz} \\ D_{yx} & D_{yy} & D_{yz} \\ D_{zx} & D_{zy} & D_{zz} \end{pmatrix} \longrightarrow \begin{pmatrix} p_{xx} & p_{xy} & p_{xz} \\ p_{yx} & p_{yy} & p_{yz} \\ p_{zx} & p_{zy} & p_{zz} \end{pmatrix} = \overline{\mathbf{P}}. \tag{3}$$

2.2. Numerical Solution Using the Finite Volume Method

Because an analytical solution to the Navier-Stokes equations is impossible with all but the most trivial models, a finite volume method is used to obtain an approximate numerical solution of the steady state, $\frac{\partial \rho v_i}{\partial t} = 0$. Each voxel is considered as a discrete control volume, and the Navier-Stokes momentum equations are integrated across it. The integrated Navier-Stokes equations are evaluated at the faces of each control volume using a hybrid differencing scheme which assumes a linear interpolation between the control volume, α, and its neighbor, β. This yields a system of linear equations equal to the dimensions of the image volume. Because of the form of this large 3-D linear system, we use the tri-diagonal matrix algorithm (TDMA), a direct method in one dimension applied iteratively over the remaining two spatial dimensions [7]. The method is iteratively applied until a user-defined convergence criterion is reached.

2.3. Computing Probable Connections

Our approach computes probable paths between two regions of interest based on the fluid velocity vector field. We approximate the ideal path through the velocity field by maximizing the cost function, $\psi(P)$ across a random sampling of possible paths.

$$\psi(P) = \frac{L_{P_0}}{L_P}\left[\int_P v(s) \cdot \hat{n}\ ds - B(P)\right] \tag{4}$$

where P is a path, v(s) is the velocity at a point s on P, $\hat{n}$ is unit tangent to s, L_P is the length of the path, L_{P_0} is the length of the shortest path between the two seed points, and B(P) is the bending energy of P, which is proportional to the path's curvature, calculated using the Frenet formulas. The cost function rewards high velocity paths while penalizing curvature.

Paths are selected using random sampling. An initial guess for the most probable path is made between the two seed points. We then iterate through a user-specified number of perturbations. At each iteration, points along the path are displaced. If the new path improves the cost function, it is used in the next iteration; otherwise, the previous path is kept.

2.4. Implementation of a Heat Equation Based Method

To compare our method to first-order approaches, we implemented a tractography method based on the first order anisotropic heat equation,

$$\frac{\partial u}{\partial t} = \nabla \cdot \overline{\mathbf{D}} \nabla u(x,t), \tag{5}$$

where u is the amount of heat. We follow an approach similar to that described by O'Donnell *et al.*[6] and solve for the steady state heat concentration ($\frac{\partial u}{\partial t} = 0$) to generate the heat flow vector field. To generate probable connection paths through the heat flow vector field, we use the approach described in Sec. 2.3, maximizing the heat flow along a path rather than the fluid velocity.

3. RESULTS

3.1. Segmentation of a Helical Digital DT-MRI Phantom

We created a digital diffusion tensor phantom using a helical tract pattern similar to the approach in [8]. We modeled the ground truth as an ideal tract with a single dominant diffusion direction at every voxel that is co-linear to the tract. Diffusion at these voxels were assumed to have values consistent with cerebral white matter, $\lambda = \{1700, 200, 200\}$ [9]. The non-tract image voxels were assumed to have diffusion values consistent with cerebral gray matter, $\lambda = \{700, 700, 700\}$ [9]. Seven images were constructed using two b values (b=0,1000) and six gradient directions. The images were taken with image volume dimensions of 128×128×75 with resolution 2×2×2 mm^3 and form the ideal signal image set. We added noise following a Rician model [10]. The level of noise added to the ideal signal image set was $\sigma = .15S_T$, where σ^2 represents the combined variance of Rician distribution and where the signal is known to span the range $[0, S_T]$.

Diffusion tensor reconstruction was then performed and lattice index and fractional anisotropy determined for each voxel in the volume. Figure 1A shows 3D renderings of the probable paths generated using our method for the phantom with relative noise magnitude of $\sigma_r^A = .15S_T$. Our method correctly segments the original helical shape, superimposed on the tracts, in the presence of noise. Figure 1B shows a segmentation result using a first order heat equation algorithm (see Sec. 2.4) on the same helical tract phantom with the same noise level as in Fig. 1A, $\sigma_r^B = .15S_T$. A comparison between the results of the two methods shows greater variability among tracts produced by the 1st order method. These variations do not correspond meaningfully with the underlying DEC and FA images.

3.2. Segmentation of the Corticospinal Tracts in Human Control DT-MRI Images

Diffusion tensor imaging data from normal human subjects were acquired using a 3T Siemens scanner with a standard quadrature head coil with the following scan parameters: image volume matrix size 128×128×75 with resolution 2×2×2 mm^3, 6 gradient directions with uniform spherical sampling, and b values 0, 600, 650, 700, and 750 s/mm^{-3}. For each subject, the set of diffusion weighted images were registered to the corresponding $b = 0$ image using a 12 parameter affine registration algorithm. Diffusion tensor reconstruction was performed and lattice index and fractional anisotropy determined for each voxel in the image.

ROIs were placed at two points in the corticospinal tracts on contralateral sides, one at the level of the basal pons and the other above the level of the corpus callosum. Figure 2 shows a 3D rendering of the probable paths which connect these ROIs, generated as

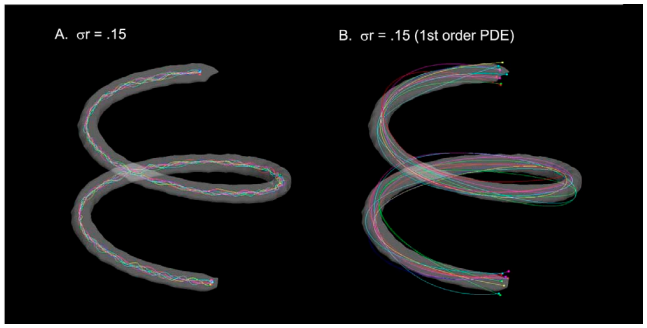

Fig. 1. Tractography results for the digital helical phantom. **A.** 3D rendering of the helical pattern with noise level $\sigma_r = .15S_T$ (see Sec. 3.1). The original helical shape is superimposed on the tracts. **B.** 3D rendering of the helical pattern using a first order heat equation algorithm on the same helical tract phantom with the same noise level as in A, $\sigma_r = .15S_T$. The original helical shape is superimposed on the tracts.

described in Sec. 2.3. These tracts (Fig. 2A) cross the midline at the level of the mid-pons (white arrow) before continuing downward in the contralateral corticospinal tract, following a strong lateral diffusion profile characteristic of the mid-pontine crossing fibers, as seen in the corresponding coronal DEC image. Fig. 2B demonstrates the ability of our method to assign likelihood to the paths generated. Here, $\psi_r > \beta$ defines the set of sampled tracts whose cost functions are above β of the maximum cost function sampled. As the threshold decreases, $\psi_r > .99$ (white) to $\psi_r > .90$ (red), the tract variability increases.

3.3. Digital Phantom Comparison of First and Second Order Methods

Our application of first-order methods to the phantom and human data described above produced comparable results to the second-order method. In this section, we describe an experiment conducted to explore the benefits of the second-order method and a possible application to DT-MRI of subjects with white matter lesions. We compared our second-order algorithm to a first-order heat-equation algorithm by applying each method to a 2D digital phantom. The phantom modeled a broad white matter tract with localized decreases in anisotropy to simulate lesion areas. Anatomically, lesions are characterized by local decreases in anisotropy, as seen in DT-MRI studies of patients with multiple sclerosis [11], and represent a disruption in the underlying white matter architecture.

As for the helical phantom above, voxels that are part of the tract are assumed to have diffusion values consistent with cerebral white matter, $\lambda = \{1700, 200, 200\}$ [9]. Non-tract image voxels are assumed to have values consistent with gray matter, $\lambda = \{700, 700, 700\}$ [9]. Four images were created using two b values ($b = 0, 1000$) and three gradient directions. The images were taken with image dimensions of 512×512 with a voxel resolution 1×1 mm^2. Two irregular ellipsoid-shaped lesions were centered at the voxel coordinates (125,250) and (350,250) and were no larger than 60 voxels in diameter in any direction. Voxels that corresponded to the non-lesioned areas of the underlying tract were assumed to have a strong major diffusion direction in the +x direction. Voxels that occupied the lesioned area were chosen to have at most one-half of the fractional anisotropy of the non-lesioned areas; this was achieved

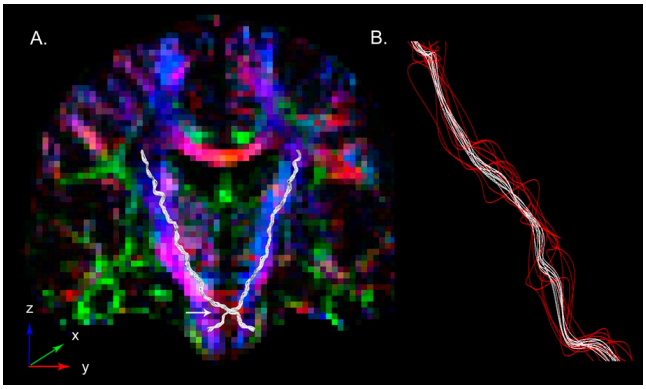

Fig. 2. Tractography results for the corticospinal tracts running from the level of pons to the corpus callosum. **A.** Full 3D-representation of the probable paths overlaid on a coronal slice of the corresponding DEC image volume for reference. Note the crossing of the tracts at the mid-pontine level (whtie arrow) before descending on the contralateral side. **B.** Enlarged portion of the paths in A, demonstrating the ability of our method to assign a relative likelihood to each tract. The tracts are color-coded to represent a relative threshold, ψ_r, where the cost function for the tract (see Sec. 2.3) is greater than ψ_r of the maximum cost function sampled. (white: $\psi_r > .99$, red: $\psi_r > .90$).

through a pseudo-random increase in the magnitude of the minor diffusion eigenvalues. This approximates the shift toward an isotropic ellipsoid characteristic in areas of white matter disruption.

We implemented a method based on the first order heat equation as described in Sec. 2.4. To facilitate a comparison with our method, we diffused an equal volume of heat/fluid from the same seed point in both models. This allowed us to use a similar metric, heat flow or fluid flow, in both models. At each voxel (i, j), we computed a normalized difference between the fluid flow and heat flow as

$$\beta_{i,j} = (f_{i,j} - h_{i,j})/(f_{i,j} + h_{i,j}), \quad (6)$$

where $f_{i,j}$ and $h_{i,j}$ denote the fluid flow and heat flow at voxel (i, j), respectively. $\beta_{i,j}$ will be at its maximum when the relative difference between $f_{i,j}$ and $h_{i,j}$ is large. Since we expect the lesioned areas to have minimal significance in any probable path, flow should be low in these areas.

Figure 3 shows a 2-D contour plot of β for all pixels in the phantom. Note that the areas of greatest difference between the methods are centered around the two lesions, where the heat flow is nearly twice the fluid flow. This is the result of the viscosity term in our method, which dampens flow in areas of low anisotropy. Our result more clearly reflects the underlying pattern, since we would expect these lesioned areas have little or no involvement in a connection between the two ROIs.

4. DISCUSSION

In this paper, we have introduced a method to estimate connectivity in DT-MRI images using a fluid mechanics model as its basis. PDE-based approaches to DT-MRI tractography are advantageous because they use the full diffusion tensor to compute metrics that can be used to assign a quantitative statistical measurement to regional connectivity. Additionally, our method can incorporate local similarity and anisotropy information into the fluid velocity vector

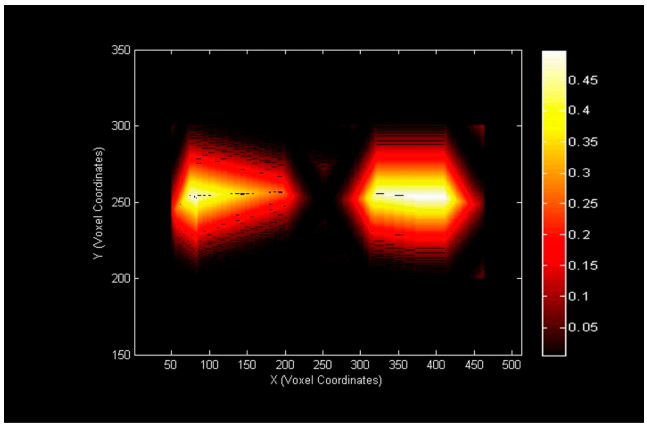

Fig. 3. Contour plot of the relative difference between the fluid flow and heat flow based connectivity maps, β, which are the segmentation result of a lesion based digital DTI phantom ($ROIs = (50, 250), (462, 250)$). Here, $\beta = (f_{i,j} - h_{i,j})/(f_{i,j} + h_{i,j})$ where $f_{i,j}$ and $h_{i,j}$ denote the fluid flow and heat flow at voxel (i,j), respectively.

field through a viscosity term. This is different from previous PDE methods, which were based on first order elliptical models [4, 6].

We validated our technique using a digital DTI phantom based on a helical pattern. Our method was able to correctly segment the underlying shape of the phantom in the presence of noise. Using normal human brain DTI data, we used our algorithm to segment the corticospinal tracts. It is well known that the corticospinal tracts cross at the level of the pons to carry motor information to the spinal cord from the contralateral motor cortex [12]. Our results confirm this, showing the most probable tracts crossing at the level of the mid-pons before descending in the contralateral tract.

Since our method is an extension of previous first order methods, we performed a comparative study of our approach and a first-order method to examine the increase in complexity of our model. We compared the two methods using a lesion phantom pattern that demonstrated how the inclusion of local anisotropy and similarity information leads to a result that more closely represents the underlying structure. Our method incorporates this information into a viscosity term, which dampens flow in areas of white matter disruption and creates an area of turbulent flow around it. Further comparative validation using other phantoms and anatomical data will be the focus of future work.

5. REFERENCES

[1] P.J. Basser, J. Mattiello, and D. Le Bihan, "Estimation of the effective self-diffusion tensor from the NMR spin echo," *J. Magnetic Resonance*, vol. 103, pp. 247–254, 1994.

[2] P.J. Basser and C. Pierpaoli, "Microstructural and physiological features of tissue elucidated by quantitative diffusion tensor MRI," *J. Magnetic Resonance*, vol. 111, pp. 209–219, 1996.

[3] S. Mori, B.J. Crain, V.P. Chacko, and P.C.M. van Zijl, "Three dimensional tracking of axonal projects in the brain by magnetic resonance imaging," *Annals of Neurology*, vol. 45, pp. 265 – 269, 1999.

[4] P.G. Batchelor, D.L.G. Hill, F. Calamante, and D. Atkinson, "Study of connectivity in the brain using the full diffusion tensor from MRI," *IPMI 2001, LNCS 2082*, pp. 121–133, 2001.

[5] P.G. Batchelor, D.L.G. Hill, D. Atkinson, F. Calamante, and A. Connelly, "Fibre-tracking by solving the diffusion-convection equation," *Proc. ISMRM*, vol. 10, 2002.

[6] L. O'Donnell, S. Haker, and C.F. Westin, "New approaches to estimation of white matter connectivity in diffusion tensor MRI: Elliptic PDEs and geodesics in a tensor-warped space," *MICCAI 2002, LNCS 2488*, pp. 459–466, 2002.

[7] H.K. Versteeg and W. Malalasekera, *An Introduction to Computational Fluid Dynamics: The Finite Volume Method*, Pearson, 1995.

[8] J. Zhang, N. Kang, and S.E. Rose, "Approximating anatomical brain connectivity with diffusion tensor MRI using kernel-based diffusion simulations," *IPMI 2005, LNCS 3565*, pp. 64–75, 2005.

[9] C. Pierpaoli, P. Jezzard, P.J. Basser, A. Barnett, and G. Di Chiro, "Diffusion tensor MR imaging of the human brain," *Radiology*, vol. 201, no. 3, pp. 637–648, 1996.

[10] H. Gudbjartsson and S. Patz, "The Rician distribution of noisy MRI data," *Mag. Reson. Med.*, vol. 34, pp. 910–914, 1995.

[11] O. Ciccarelli, D.J. Werring, C.A.M. WheelerKingshott, G.J. Barker, G.J.M. Parker, A.J. Thompson, and D.H. Miller, "Investigation of MS normal-appearing brain using diffusion tensor MRI with clinical correlations," *Neurology*, vol. 56, pp. 926–933, 2001.

[12] J. Nolte, *The Human Brain: An Introduction to Its Functional Anatomy*, Mosby, 5th edition, 2002.